Journal of the Korean Physical Society, Vol. 63, No. 4, August 2013, pp. 943∼950

Generation of Nonclassical Narrowband Photon Pairs from a Cold Rubidium Cloud

Young-Wook Cho,* Kwang-Kyoon Park, Jong-Chan Lee and Yoon-Ho Kim†
Department of Physics, Pohang University of Science and Technology (POSTECH), Pohang 790-784, Korea

(Received 17 January 2013, in final form 25 February 2013)

We report the generation of nonclassical narrowband photon pairs via the spontaneous four-wave mixing process in a cold Rubidium (^{87}Rb) cloud prepared in a magneto-optical trap. The generated photon pairs exhibit strong violation of the Cauchy-Schwarz inequality by a factor of 625 ± 45, confirming nonclassical correlation between the photons. The biphoton wave packets, measured for several different experimental conditions, are in good agreement with the theoretical results.

PACS numbers: 42.50.Gy, 32.80.-t, 42.50.Dv, 42.65.Lm
Keywords: Entangled photon pair, Electromagnetically-induced transparency, Spontaneous four-wave mixing
DOI: 10.3938/jkps.63.943

I. INTRODUCTION

The entangled photon source is an essential resource not only for research on the foundations of quantum physics, but also for quantum information science. Since the late 1980's, spontaneous parametric down-conversion (SPDC) in a non-centrosymmetric crystal with $\chi^{(2)}$ nonlinearity has been the main source of entangled photon pairs [1]. While SPDC still remains the best way to produce entangled photon pairs experimentally and is being used predominantly in photonic quantum information research, the intrinsic broadband ($\sim$ THz) nature (hence, very short coherence time on the order $\sim$ ps) of SPDC photons limits certain important applications. For instance, the biphoton waveform of conventional SPDC photon pairs cannot be directly resolved because even the state-of-the-art photon counting systems have timing resolutions on the order of several hundreds of ps [2–4]. This then limits the direct time-domain biphoton waveform manipulation for quantum information processing [5–7]. Also, the broadband nature of SPDC is not well suited for strong atom-photon interaction, thereby causing difficulties in quantum information transfer between flying qubits and atomic qubits [8, 9], which is essential for long-distance quantum communication [10, 11], atomic-ensemble-based quantum memories [12–14], *etc.*

In recent years, there has been great interest in generating narrowband entangled photon pairs. One straightforward way to generate narrowband biphotons is to place the SPDC medium in an optical cavity. At pump powers far below the optical parametric oscillator (OPO) threshold, the spontaneous nature of biphoton generation is maintained while the emission bandwidth of the biphoton is greatly reduced [15,16]. Significant improvement of the biphoton generation rate has been observed and biphotons with bandwidths of several MHz can be routinely accomplished by using the cavity-enhanced SPDC process [17–21]. However, the biphoton waveform (typically Lorentzian), which is primarily determined by the cavity, is not readily controllable, and the periodic nature of cavity emission can cause further complications.

Nonclassical photon pairs have also been generated in an atomic ensemble by using the so-called "write-read" pulse technique [22–25]. Although the photon pairs generated via the "write-read" pulse technique exhibit strong nonclassical correlation, there is no energy-time entanglement between the photons because the successive spontaneous Raman scattering processes are time-separated processes [25].

Recently, generation of paired photons has been observed by using the spontaneous four-wave mixing (SFWM) process in a cold atomic ensemble where the $\chi^{(3)}$ nonlinear interaction is enhanced greatly by electromagnetically-induced transparency (EIT) [7, 26–30]. Note that the biphoton generation in a cold atomic ensemble is similar in its mechanism to that in an optical fiber as both utilize the SFWM process. However, the cold-atom SFWM process offers very narrowband biphotons, as well as many control parameters for biphoton waveform engineering [31–33].

In this paper, we report an experimental study on narrowband nonclassical photon pairs generated via the

*E-mail: choyoungwook81@gmail.com
†E-mail: yoonho72@gmail.com

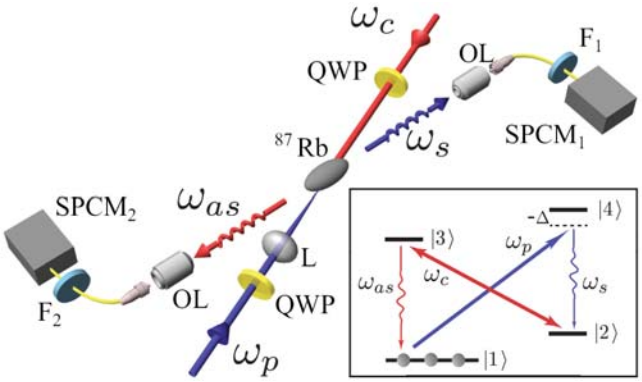

Fig. 1. (Color online) Sketch of the experimental setup. The pump (ω_p) and the coupling (ω_c) laser beams, via the SFWM process in the cold ^{87}Rb atom cloud, create a Stokes (ω_s) photon and an anti-Stokes (ω_{as}) photon. The inset shows the ^{87}Rb energy level diagram for SFWM, where $|1\rangle = |5S_{1/2}(F=1)\rangle$, $|2\rangle = |5S_{1/2}(F=2)\rangle$, $|3\rangle = |5P_{1/2}(F'=2)\rangle$, and $|4\rangle = |5P_{3/2}(F'=2)\rangle$. SPCM is the single photon counting module, L is the lens, QWP is the quarter-wave plate, OL is the objective lens, and F is the solid etalon filter.

SFWM process in a cold ^{87}Rb atomic ensemble prepared in a magneto-optical trap (MOT). We show experimentally that the generated photon pairs exhibit nonclassical quantum correlation by observing strong violation of the Cauchy-Schwarz inequality of the correlation functions by a factor of 625 ± 45. We also show that the measured biphoton wave packets are in good agreement with the theoretical results.

This paper is organized as follows: In Sec. II, we briefly describe the theory behind the biphoton state of SFWM in a double Λ-type EIT system. Section III is devoted to the associated experiments. In particular, we describe the process for preparing the cold atomic ensemble and the experimental sequence in Sec. III. 1. The main results, the demonstration of nonclassical biphoton generation, are described in Sec. III. 2. Finally, we summarize our observations and conclude in Sec. IV.

II. THEORY

Let us start by describing the SFWM process in an atomic ensemble prepared by using the experimental schematic illustrated in Fig. 1. When pump (ω_p) and coupling (ω_c) fields are applied to a cold ^{87}Rb cloud with length L, Stokes (ω_s) and anti-Stokes (ω_{as}) photon pairs are generated via the SFWM process. For simplicity, we consider a simple four-level double Λ-type energy level structure, as shown in the inset of Fig. 1. Initially, all atoms are populated in the ground state $|1\rangle$. A strong coupling field (ω_c) resonant with the $|2\rangle \leftrightarrow |3\rangle$ transition not only enhances the third-order nonlinear interaction but also creates the EIT window for the anti-Stokes photon (ω_{as}). In order to maintain a low parametric gain, we set the pump laser (ω_p) power to be relatively weaker than that of the coupling laser and to be red-detuned by Δ from the $|1\rangle \leftrightarrow |4\rangle$ transition.

In the interaction picture, the effective Hamiltonian for the SFWM process is given by [34]

$$\hat{H}_I = \frac{\epsilon_0 A}{4} \int_{-L/2}^{L/2} dz\ \chi^{(3)} E_p^{(+)} E_c^{(+)} \hat{E}_s^{(-)} \hat{E}_{as}^{(-)} + h.c.,$$

where A is the single-mode cross-sectional area, $\chi^{(3)}$ is the third-order nonlinear susceptibility, and $h.c.$ denotes the hermitian conjugate. The coupling laser field $E_c^{(+)}$ and the pump laser field $E_p^{(+)}$ are treated classically and are given as

$$\begin{aligned} E_p^{(+)}(z,t) &= E_p\, e^{i(k_p z - \omega_p t)}, \\ E_c^{(+)}(z,t) &= E_c\, e^{i(-k_c z - \omega_c t)}, \end{aligned}$$

where E_p and E_c are the field amplitudes. The Stokes field $E_s^{(-)}$ and the anti-Stokes field $E_{as}^{(-)}$ are treated quantum mechanically and are given as

$$\begin{aligned} \hat{E}_s^{(-)}(z,t) &= \int d\omega_s\, \mathcal{E}_s\, \hat{a}_s^\dagger(\omega_s)\, e^{-i(k_s z - \omega_s t)}, \\ \hat{E}_{as}^{(-)}(z,t) &= \int d\omega_{as}\, \mathcal{E}_{as}\, \hat{a}_{as}^\dagger(\omega_{as})\, e^{-i(-k_{as} z - \omega_{as} t)}, \end{aligned}$$

where $\hat{a}_s^\dagger$ and $\hat{a}_{as}^\dagger$, respectively, are the photon creation operators for the Stokes and the anti-Stokes photons. The field amplitude is defined as $\mathcal{E}_j = \sqrt{\frac{\hbar\omega_j}{\pi c \epsilon_0 A}}$ ($j = s, as$), where c and ϵ_0 are the speed of light and the vacuum permittivity, respectively.

Using the first-order perturbation theory, the biphoton state of SFWM is calculated to be [34]

$$\begin{aligned} |\Psi\rangle &= C \int d\omega_{as}\ \chi^{(3)}(\omega_{as}, -\omega_{as})\, \mathrm{sinc}\left(\frac{\Delta k L}{2}\right) \\ &\quad \times \hat{a}_s^\dagger(\omega_p + \omega_c - \omega_{as}) \hat{a}_{as}^\dagger(\omega_{as}) |0\rangle. \end{aligned}$$

All slowly-varying terms and constants are grouped into C and $\Delta k = k_p - k_c - k_s + k_{as}$ is the phase mismatch term.

Similarly to the SPDC case [35,36], the biphoton amplitude for the SFWM photon pair can be defined as

$$\Psi(t_{as}, t_s) = \langle 0 | \hat{a}_{as}(t_{as}) \hat{a}_s(t_s) | \Psi \rangle,$$

where t_{as} and t_s, respectively, refer to the detection times for anti-Stokes and Stokes photons. The biphoton waveform shape can be visualized with Glauber's second-order correlation function, $G^{(2)}(\tau = t_{as} - t_s) = |\Psi(t_{as}, t_s)|^2$, and is calculated to be [34]

$$\begin{aligned} \Psi(t_{as}, t_s) &= \frac{C}{2\pi} \int d\omega_{as}\ \chi^{(3)}(\omega_{as}, -\omega_{as})\, \Phi(\omega_{as}) \\ &\quad \times e^{-i\omega_{as}\tau} e^{-i(\omega_c + \omega_p) t_s}, \end{aligned} \tag{1}$$

where the longitudinal phase-matching function $\Phi(\omega_{as})$ is given as

$$\Phi(\omega_{as}) = \mathrm{sinc}(\Delta k L/2)\, e^{i(k_{as} + k_s) L/2}.$$

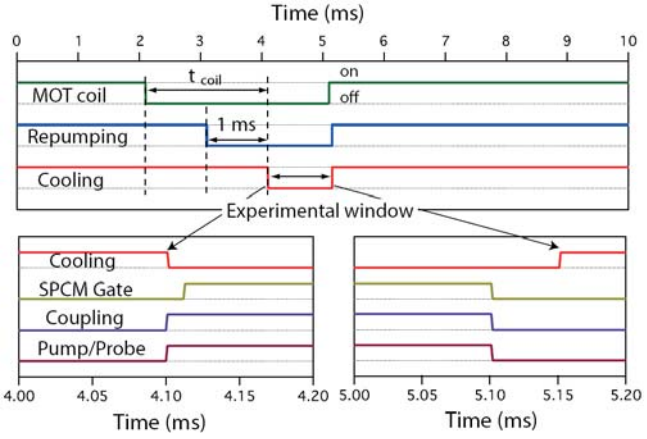

Fig. 2. (Color online) Timing sequence for the SFWM biphoton generation using the cold atom cloud. The cooling and the repumping lasers prepare a cold ^{87}Rb cloud and are turned off during the experimental window. The repumping laser is turned off 1 ms before turning off the cooling laser so that the cold atom cloud is prepared at the $F = 1$ ground state. The quadrupole MOT magnetic field is switched off $t_{\rm coil}$ before turning off the cooling laser. During the experimental window of 105 μs, the coupling and the pump beams are turned on, and the SPCM's are gated to turn on to detect the Stokes and anti-Stokes biphotons. The whole experimental procedure is repeated at a repetition rate of 0.1 kHz. See the text for details.

From Eq. (1), clearly, the biphoton waveform shape is determined by the third-order nonlinear susceptibility $\chi^{(3)}(\omega_{as})$ and the phase-matching function $\Phi(\omega_{as})$.

Mathematically, the convolution of $\mathcal{F}[\chi^{(3)}(\omega_{as})]$ and $\mathcal{F}[\Phi(\omega_{as})]$ determines the biphoton waveform shape, where $\mathcal{F}[...]$ denotes the Fourier transform. The nonlinear optical susceptibility $\chi^{(3)}(\omega)$ for the four-level double Λ-type EIT system with the ground state approximation, *i.e.*, most of the atoms are in the ground state $|1\rangle$, has been well studied and is given as [34]

$$\chi^{(3)}(\omega) = \frac{N\mu_{13}\,\mu_{32}\,\mu_{24}\,\mu_{41}/(\epsilon_0\hbar^3)}{(\Delta + i\gamma_{14})[|\Omega_c|^2 - 4(\omega + i\gamma_{13})(\omega + i\gamma_{12})]},$$

where μ_{ij} is the electric dipole matrix element, γ_{ij} is the dephasing rate, N is the number density of the atoms, $\Delta = \omega_p - \omega_{41}$ is the pump detuning, and Ω_c is the Rabi frequency due to the coupling laser.

The phase-matching function $\Phi(\omega_{as})$ can be approximated by using the well-known relation

$$k(\omega) = k^0\sqrt{1+\chi(\omega)} \simeq k^0\left[1 + \frac{1}{2}\chi(\omega)\right],$$

where k^0 is the vacuum wave number and $\chi(\omega)$ is the linear optical susceptibility of the medium. The phase-matching function $\Phi(\omega_{as})$ is then given as

$$\Phi(\omega_{as}) \simeq \mathrm{sinc}\left[\frac{k^0_{as}L}{4}\chi_{as}(\omega_{as})\right]\exp\left(i\frac{k^0_{as}L}{4}\chi_{as}(\omega_{as})\right),$$

where we have used the approximation $\chi_s \simeq 0$ for the weak pump limit at low parametric gain, $|\Omega_p|^2 \ll \Delta^2$, as implied in the equation for $\chi_s(\omega)$ below. Note that the irrelevant phase term $e^{i(k^0_s + k^0_{as})L/2}$ has been omitted in the above equation. The linear optical susceptibilities for the Stokes and the anti-Stokes photons for the four-level double Λ-type EIT system are given as [34]

$$\chi_s(\omega) = \frac{N|\mu_{24}|^2(\omega - i\gamma_{13})/(\epsilon_0\hbar)}{|\Omega_c|^2 - 4(\omega - i\gamma_{13})(\omega - i\gamma_{12})}\frac{|\Omega_p|^2}{\Delta^2 + \gamma_{14}},$$

$$\chi_{as}(\omega) = \frac{4N|\mu_{13}|^2(\omega + i\gamma_{12})/(\epsilon_0\hbar)}{|\Omega_c|^2 - 4(\omega + i\gamma_{13})(\omega + i\gamma_{12})},$$

where Ω_p is the Rabi frequency due to the pump laser. Given the linear and the nonlinear optical susceptibilities, we can then evaluate the biphoton waveform shape by numerically integrating Eq. (1). A more detailed description of the theory of SFWM in a cold atom cloud can be found in Refs. [27,34,37].

III. EXPERIMENT

1. Preparation of a Cold ^{87}Rb Ensemble

The cold ^{87}Rb atomic ensemble is prepared by laser cooling the thermal vapor and trapping it in a 3D MOT. The cooling laser is spatially filtered by using a single-mode optical fiber and divided into three pairs of retro-reflecting beams with diameters of 1 inch. The frequency of the cooling laser is red-detuned at 20 MHz below the $|5S_{1/2}(F = 2)\rangle \rightarrow |5P_{3/2}(F' = 3)\rangle$ transition. The repumping laser is tuned to the $|5S_{1/2}(F = 1)\rangle \rightarrow |5P_{3/2}(F' = 2)\rangle$ resonance and pumps atoms in the $|5S_{1/2}(F = 1)\rangle$ ground state back into the $|5S_{1/2}(F = 2)\rangle$ ground state. Both the cooling and the repumping lasers are frequency-stabilized by using saturation absorption spectroscopy. The quadrupole MOT's magnetic field is generated by using a pair of anti-Helmholtz coils, and the generated magnetic-field gradient is 10 G/cm. Also, in order to cancel any stray magnetic fields from the earth and the background electronics, we used three pairs of Helmholtz coils.

Figure 2 shows the timing sequence of the experiment. Both the cooling and the repumping lasers are turned off during the 105-μs experimental window. By switching off the repumping laser 1 ms before the start of the experimental window, the cold ^{87}Rb atomic ensemble is prepared in the $|5S_{1/2}(F = 1)\rangle$ ground state. The whole sequence is then repeated at a repetition period of 10 ms; *i.e.*, the cold atom cloud is recaptured every 10 ms with an experimental window of 105 μs.

We first characterized the cold atomic ensemble by measuring the absorption and the EIT spectra with a 100-μs probe pulse during the experimental window. The frequency of the probe laser was swept over 80 MHz

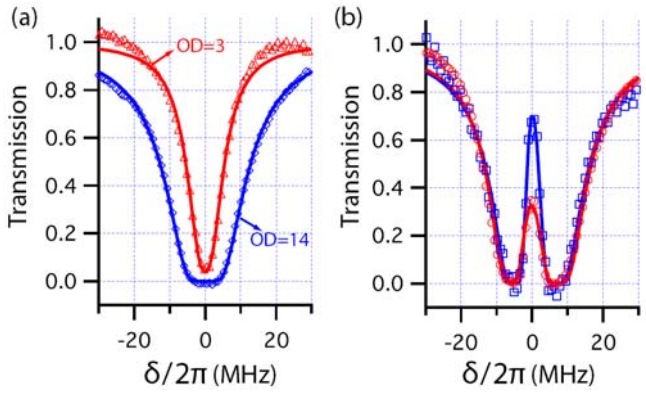

Fig. 3. (Color online) Experimental transmission spectra. (a) Two-level absorption spectra for two different OD values. Solid lines are theoretical curves due to Eq. (2) with $\Omega_c = 0$. (b) Λ-type three-level EIT spectra for two different γ_{12} values. Solid lines are theoretical curves due to Eq. (2) with fitting parameter sets $\{\mathcal{D} = 13$, $\gamma_{12} = 2\pi \times 0.28$ MHz, $\gamma_{13} = 2\pi \times 3$ MHz, $\Omega_c = 2\pi \times 11.13$ MHz$\}$ for blue open rectangles and $\{\mathcal{D} = 12$, $\gamma_{12} = 2\pi \times 1.5$ MHz, $\gamma_{13} = 2\pi \times 3$ MHz, $\Omega_c = 2\pi \times 12.84$ MHz$\}$ for the red open circles.

near the $|5S_{1/2}(F = 1)\rangle \rightarrow |5P_{1/2}(F' = 2)\rangle$ transition within the 100-μs probe's pulse width. For measuring the EIT spectra, a coupling laser locked to the $|5S_{1/2}(F = 2)\rangle \rightarrow |5P_{1/2}(F' = 2)\rangle$ transition was also applied during the experimental window. See the inset in Fig. 1 for the relevant energy level diagram. Both the probe and the coupling lasers have the same circular polarization to create the parallel EIT channel. To minimize the effect of the laser's linewidth on the EIT spectra, the coupling and the probe lasers were derived from the same laser, effectively phase-locking both lasers [38].

The experimental data for the two-level absorption measurement and the Λ-type three-level EIT spectrum measurement are shown in Fig. 3. The optical depth (OD) of the cold atom cloud was derived from the experimental data by using the three-level theoretical EIT transmission spectrum [39]

$$T(\delta) = \exp\left(-\mathrm{Im}\left[\frac{4\mathcal{D}\,\gamma_{13}\,(\delta + i\gamma_{12})}{|\Omega_c|^2 - 4(\delta + i\gamma_{13})(\delta + i\gamma_{12})}\right]\right), \quad (2)$$

where δ is the frequency detuning of the applied probe laser, γ_{12} is the ground-state dephasing rate, and the optical depth is defined as $\mathcal{D} = N\sigma_{13}L$, with $\sigma_{13} = c|\mu_{13}|^2/\epsilon_0\hbar\gamma_{13}\omega_{13}$ being the atomic cross-section at the $|5S_{1/2}(F = 1)\rangle \rightarrow |5P_{1/2}(F' = 2)\rangle$ transition. The above relation reduces to the two-level absorption spectrum when the coupling beam is turned off, *i.e.*, $\Omega_c = 0$. The maximum OD of our 3D MOT was measured to be $\mathcal{D} = 16$ and could be varied by changing the electric current applied to the Rb dispenser and the power of the repumping laser.

In the presence of the MOT quadrupole magnetic field (MOT coil turned on), we were able to achieve a ground-state dephasing rate γ_{12} down to $2\pi \times 0.5$ MHz by cancelling the stray magnetic fields with three pairs of Helmholtz coils. To further reduce γ_{12}, we switched off the MOT coil by using a fast metal-oxide-semiconductor field-effect transistor (MOSFET) switching circuit [40]. As shown in Fig. 4, by increasing the MOT coil's turn-off delay, γ_{12} could be reduced down to $2\pi \times 0.15$ MHz. However, when the MOT coil is turned off too long, atoms start to diffuse out from the trapping region and this causes the OD to decrease. Obviously, there is a certain trade-off between a high OD and a low γ_{12}, and this affects the biphoton waveform shape. In this paper, we have also studied their effects on the biphoton waveform shape as we shall show in Sec. III. 2.

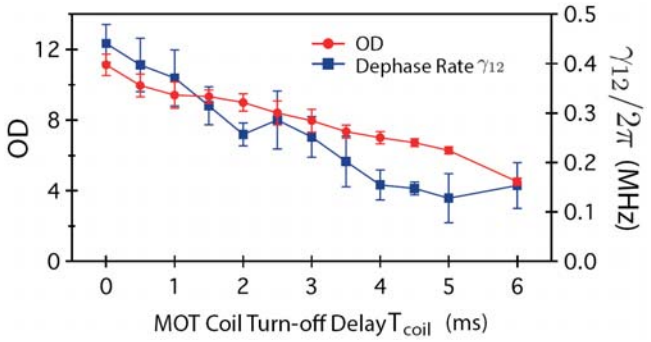

Fig. 4. (Color online) Optical depth (OD) and ground-state dephasing rate γ_{12} as a function of the MOT coil turn-off delay T_{coil}. The experiment is repeated at a 10-ms repetition period.

2. Nonclassical Narrowband Photon Pair Generation in the 3D MOT via SFWM

We now discuss the generation of narrowband biphotons from the cold atomic ensemble by using the scheme depicted in Fig. 1. The frequency of the coupling laser (ω_c) is locked to the $5S_{1/2}|F = 2\rangle \rightarrow 5P_{1/2}|F' = 2\rangle$ transition, and the coupling laser has a $1/e^2$ diameter of 2.65 mm. The optical power of the coupling laser is approximately 20 mW, which corresponds to the Rabi frequency $\Omega_c \approx 2\pi \times 58$ MHz. The pump laser (ω_p) is frequency locked to $2\pi \times 63$ MHz below (*i.e.*, red-detuned) the $|5S_{1/2}(F = 1)\rangle \rightarrow |5P_{3/2}(F' = 2)\rangle$ transition and is focused to a $1/e^2$ diameter of 216 μm by using a lens with a 500-mm focal length to increase the collection efficiency of the Stokes and the anti-Stokes photons into single-mode fibers [41]. The optical power of the pump laser is kept less than 75 μW, with a corresponding Rabi frequency of $\Omega_p \approx 2\pi \times 30$ MHz. The polarizations of the coupling and the pump lasers are σ^+ and σ^-, respectively.

When the cold ^{87}Rb atomic ensemble is illuminated by the counter-propagating coupling and pump beams, Stokes (ω_s) and anti-Stokes (ω_{as}) photons are generated

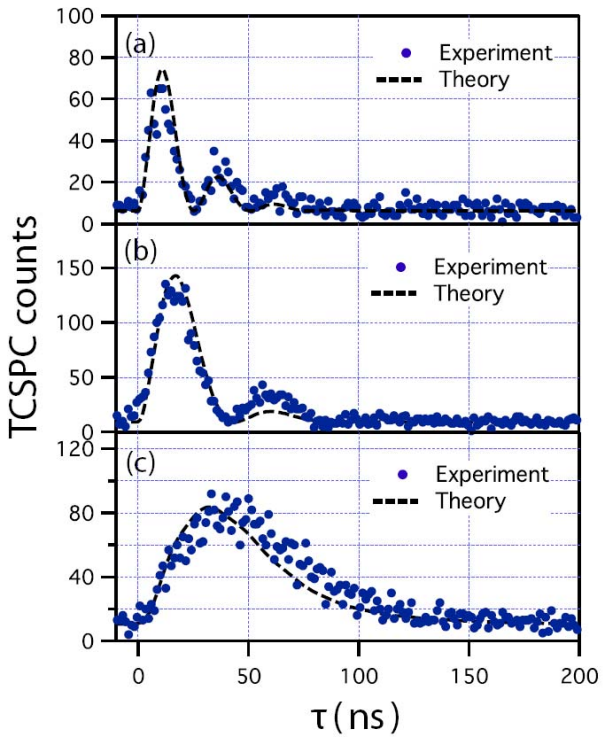

Fig. 5. (Color online) Biphoton waveform shape at OD $\mathcal{D} = 6.3$ for different coupling laser Rabi frequencies: (a) $\Omega_c = 2\pi \times 40$ MHz, (b) $\Omega_c = 2\pi \times 24$ MHz, and (c) $\Omega_c = 2\pi \times 8.7$ MHz. The ground-state dephasing rate is $\gamma_{12} = 2\pi \times 0.57$ MHz. The measured biphoton shapes are in good agreement with the theory. TCSPC counts are measured for 600 s.

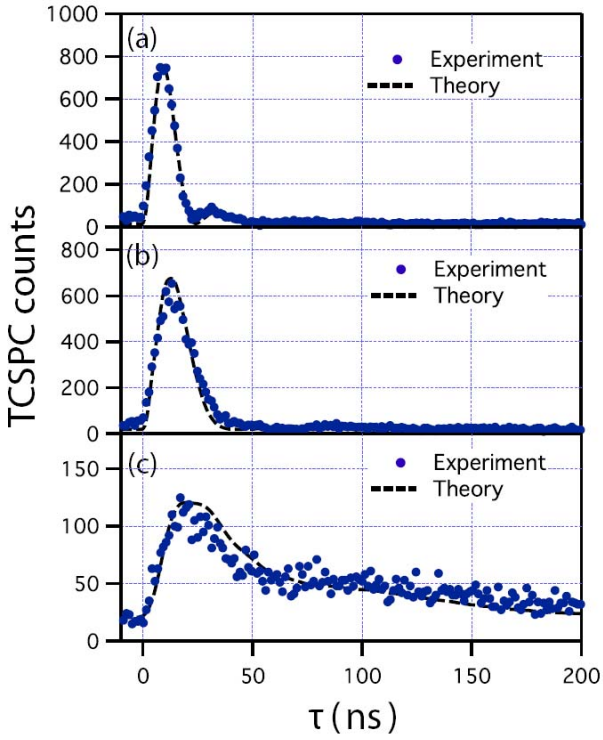

Fig. 6. (Color online) Biphoton waveform shape at OD $\mathcal{D} = 13.8$ for different coupling laser Rabi frequencies: (a) $\Omega_c = 2\pi \times 43.6$ MHz, (b) $\Omega_c = 2\pi \times 28.8$ MHz, (c) $\Omega_c = 2\pi \times 8.7$ MHz. The ground-state dephasing rate is $\gamma_{12} = 2\pi \times 0.65$ MHz. The measured biphoton shapes are in good agreement with the theory. TCSPC counts are measured for 600 s.

in opposite directions via the SFWM process. In order to spatially filter Stokes and anti-Stokes photons from the strong pump and coupling laser beams, we collect the Stokes and the anti-Stokes photons at an angle of 3° from the pump and the coupling beams. The SFWM photon pairs are collected into single-mode fibers with objective lenses (Newport M-10X; 16.5-mm focal length, 7.5-mm clear aperture, and 0.25 numerical aperture). To ensure that correlated photon pairs are collected, we carefully align the fiber couplers for Stokes and anti-Stokes modes such that a laser beam emitted from one is coupled into the other with a coupling efficiency better than 70%.

To further isolate the Stokes and the anti-Stokes photons from the strong pump and the coupling lasers, we use a pair of temperature-tuned solid etalons (470-MHz full-width-at-half-maximum transmission bandwidth; 21 GHz free spectral range). The peak transmission of the etalon itself was measured to be 70%. The SFWM photons are then coupled into multi-mode fibers and detected by using single-photon counting modules (Perkin Elmer SPCM-AQRH-13FC). The overall transmission of the etalon filter system (including the coupling efficiency into the multi-mode fiber, the fiber connection losses, and the etalon transmission) was measured to be 40%.

As shown in the experimental timing sequence in Fig. 2, Stokes and anti-Stokes photons are detected only during the 98-μs SPCM gating window within the 105-μs experimental window. The measurement is then repeated at a 10-ms repetition period for which the whole experiment is repeated. The biphoton waveform shape is observed with a timing module (SensL; HRM-TDC) operated in the time-correlated single-photon counting (TCSPC) mode. The timing resolution of the TCSPC was set at 1.3 ns. Because the biphoton coherence time of the SFWM biphoton is much greater than the TCSPC timing resolution, the TCSPC histogram measured as a function of $\tau = t_{as} - t_s$ directly reflects the shape of the biphoton waveform.

Figures 5 and 6 show the measured biphoton waveform shapes. With fixed OD at $\mathcal{D} = 6.3$ and 13.8 (see Fig. 5 and Fig. 6, respectively), we varied the coupling Rabi frequency Ω_c. As expected, the Stokes photons are always detected earlier (*i.e.*, born earlier) than the anti-Stokes photons. The experimental data are in excellent agreement with the theoretical results obtained by numerically integrating Eq. (1) with the parameters corresponding to each experiment. The theoretical results are vertically scaled to account for the measurement time and shifted upward to handle accidental coincidence counts.

As inferred from Eq. (1), the biphoton waveform is

determined by both $\chi^{(3)}(\omega_{as})$ and $\Phi(\omega_{as})$. We may define three important characteristic times that affect the biphoton waveform. The first characteristic time is the maximum group delay for the anti-Stokes photon and is given as

$$\tau_g \simeq \frac{2\gamma_{13}\mathcal{D}}{|\Omega_c|^2 + 4\gamma_{13}\gamma_{12}}.$$

Note that the dispersion property determines $\Phi(\omega_{as})$ so that the bandwidth of the phase-matching function is $\Delta\Phi(\omega_{as}) \propto 1/\tau_g$. The second and third characteristic times are the effective dephasing time τ_e and the effective coupling Rabi time τ_r. They are relevant to $\chi^{(3)}(\omega_{as})$ and are defined as [7]

$$\begin{aligned} \tau_e &= 1/(\gamma_{13}+\gamma_{12}), \\ \tau_r &= 2\pi/\sqrt{|\Omega_c|^2 - (\gamma_{13}-\gamma_{12})^2}. \end{aligned}$$

The biphoton waveform is determined by competition between τ_g, τ_e, and τ_r.

From the given experimental conditions, we estimate an effective dephasing time of about $\tau_e = 45$ ns in our experiment. The estimated group delays τ_g are (a) 3.77 ns, (b) 10.4 ns, and (c) 73.4 ns for Fig. 5 and (a) 6.89 ns, (b) 15.7 ns, and (c) 157 ns for Fig. 6. The effective coupling Rabi times τ_r are (a) 25 ns, (b) 42 ns, and (c) 120 ns for Fig. 5 and (a) 23 ns, (b) 35 ns, and (c) 119 ns for Fig. 6.

When τ_g is smaller than τ_e or τ_r, $\Phi(\omega_{as})$ has larger bandwidth than $\chi^{(3)}(\omega_{as})$. In this case, we can treat $\Phi(\omega_{as})$ as a constant; thus, the biphoton waveform is mainly determined by $\chi^{(3)}(\omega_{as})$. In this regime, the biphoton correlation function shows a damped oscillatory behavior, where the oscillation period is determined by τ_r [7]. Clearly, the biphoton shape is controlled by the value of Ω_c, which determines both τ_g and τ_r. The damped oscillatory behaviors for the condition $\tau_g < \{\tau_e \text{ or } \tau_r\}$ are clearly demonstrated in Fig. 5, Fig. 6(a), and Fig. 6(b), where the oscillation periods coincide with τ_r. Note that, for the case of $\tau_e < \tau_r$, see Fig. 5(c), the oscillation is washed out due to the short dephasing time. It is also clear from Fig. 5(a) and Fig. 6(a) that the damped oscillatory behavior is more clearly visible with a lower OD as a higher OD decreases the dephasing time τ_e. Therefore, even in the damped Rabi oscillation regime in which $\chi^{(3)}$ mainly determines the biphoton waveform, τ_g plays some role in determining the biphoton waveform.

Let us now consider the case in which the maximum group delay for the anti-Stokes photon is larger than the effective coupling Rabi time, $\tau_g > \tau_r$. In this regime, the phase-matching function $\Phi(\omega_{as})$ plays the dominant role in determining the biphoton waveform, and the oscillation behavior completely disappears. Thus, the coherence time of the biphoton is mainly determined by τ_g [7] and, as shown in Fig. 6(c), the biphoton coherence times almost coincide with τ_g.

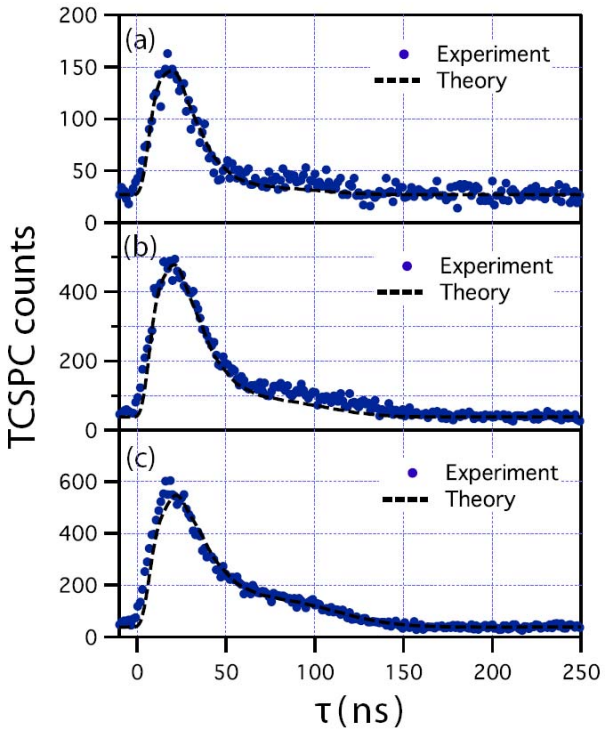

Fig. 7. (Color online) Biphoton waveform shape at OD $\mathcal{D} = 13.2$ for different ground-state dephasing rates: (a) $\gamma_{12} = 2\pi \times 1.98$ MHz, (b) $\gamma_{12} = 2\pi \times 1.13$ MHz, and (c) $\gamma_{12} = 2\pi \times 0.33$ MHz. The coupling laser Rabi frequency is $\Omega_c = 2\pi \times 11.9$ MHz. The measured biphoton shapes are in good agreement with the theory. TCSPC counts are measured for 1200 s.

We have also observed the dependence of the biphoton waveform shape on the ground-state dephasing rate γ_{12} (see Fig. 7). The OD was set at $\mathcal{D} = 13.2$, and the coupling laser Rabi frequency was set at $\Omega_c = 2\pi \times 11.9$ MHz. The ground-state dephasing rate γ_{12} was adjusted by changing the electric current through the three pairs of compensating Helmholtz coils or by switching off the MOT coil. For instance, $\gamma_{12} = 2\pi \times 0.33$ MHz was obtained by setting the MOT's coil turn-off delay at $T_{coil} = 2$ ms. As shown in Fig. 7, as γ_{12} is decreased, the biphoton coherence time becomes bigger. This clearly indicates that γ_{12} can be used to control the biphoton waveform shape.

Finally, to verify that the SFWM photon pairs have nonclassical quantum correlation, we tested the Cauchy-Schwarz inequality for the second-order correlation measurements. It is well-known that, for classical light such as thermal light and laser light, the Cauchy-Schwarz inequality

$$\mathcal{R} = \frac{\left[g^{(2)}_{s,as}(\tau)\right]^2}{g^{(2)}_{s,s}(0)\; g^{(2)}_{as,as}(0)} \leq 1$$

is satisfied [22, 23]. Here, $g^{(2)}_{s,as}(\tau)$ is the normalized

Table 1. Maximum $g^{(2)}_{s,as}(\tau)$ values and corresponding $\mathcal{R}$ values. The Cauchy-Schwarz inequality is clearly violated.

	Figure 5	Figure 6	Figure 7	
$g^{(2)}_{s,as}(\tau)$	10 ± 1	50 ± 2	6 ± 1	(a)
$\mathcal{R}$	25 ± 7	625 ± 45	9 ± 1	
$g^{(2)}_{s,as}(\tau)$	15 ± 1	34 ± 1	13 ± 1	(b)
$\mathcal{R}$	56 ± 9	289 ± 23	42 ± 4	
$g^{(2)}_{s,as}(\tau)$	9 ± 1	6 ± 1	16 ± 1	(c)
$\mathcal{R}$	20 ± 4	9 ± 2	64 ± 5	

second-order cross-correlation function, and $g^{(2)}_{s,s}$ ($g^{(2)}_{as,as}$) is the normalized second-order auto-correlation function for the Stokes (anti-Stokes) photon. The normalized second-order cross-correlation function $g^{(2)}_{s,as}(\tau)$ can be obtained by normalizing the TCSPC data to the accidental noise level, $g^{(2)}_{s,as}(\infty)$. For instance, we obtained the maximum cross-correlation $g^{(2)}_{s,as}(\tau) = 50 \pm 2$ at $\tau = 10$ ns for Fig. 6(a). Thus, the corresponding Cauch-Schwarz inequality factor $\mathcal{R} = 625 \pm 45 \nleq 1$ is obtained using the fact that the auto-correlation functions for the spontaneously-emitted Stokes and anti-Stokes photons exhibit the thermal light photon statistics (*i.e.*, $g^{(2)}_{s,s} = g^{(2)}_{as,as} \simeq 2$).

All experimental results in Figs. 5-7 violate the Cauchy-Schwarz inequality, as summarized in Table. I, and this clearly shows that the photon pairs exhibit strong non-classical correlation. The degree of violation (hence, the degree of nonclassical correlation) is determined by the SFWM photon pair flux, which is proportional to the pump power, and by the accidental coincidence count rate, which is proportional to the square of the pump power. Thus, it should be possible to further increase $\mathcal{R}$ by reducing the pump power at the expense of reduced photon pair flux.

IV. SUMMARY

We have presented a detailed study on generation of the narrowband nonclassical photon pairs in a cold atomic ensemble via the SFWM process. First, we have discussed the theory of the SFWM process in an atomic ensemble for nonclassical photon pair generation. Next, we have described our experimental results for photon pair generation in a cold atom ensemble prepared in a 3D MOT. The biphoton waveform shape observed in the experiment agreed well with the theoretical results. We have also shown that the SFWM photon pairs have nonclassical quantum correlation by demonstrating that the Cauchy-Schwarz inequality is violated. The strong violation of the Cauchy-Schwarz inequality implies that the SFWM photon pair is, indeed, energy-time entangled although it should be noted that a direct test of entanglement requires, for instance, Bell violation, an entanglement witness measurement, or a partial transposition. We are presently working toward a direct experimental demonstration of energy-time entanglement between the SFWM photon pair. The MOT-based narrowband entangled photon source is expected to play important roles in photonic quantum information research, in particular, for atom-photon quantum interface, quantum memories, heralded single-photon generation, quantum non-demolition measurements, *etc.*

ACKNOWLEDGMENTS

We would like to thank Shengwang Du, Hoonsoo Kang, Jung-Bog Kim, Han-Seb Moon, Jianming Wen, and Hoon Yu for many fruitful discussions. This work was partially supported by the National Research Foundation of Korea (Grants No. 2011-0021452 and No. 2013R1A2A1A01006029). Y.-W. C. and J.-C. L. acknowledge support from the National Junior Research Fellowship (Grants No. 2011-0010895 and No. 2012-000741, respectively). K-K.P. acknowledges support from Global Ph. D. Fellowship by National Research Foundation of Korea (Grant No. 2011-0030856).

REFERENCES

[1] D. N. Klyshko, *Photons and Nonlinear Optics* (Gordon & Breach, New York, 1988).
[2] O. Kuzucu, F. N. C. Wong, S. Kurimura and S. Tovstonog, Phys. Rev. Lett. **101**, 153602 (2008).
[3] A. V. Sergienko, Y. H. Shih and M. H. Rubin, J. Opt. Soc. Am. B **12**, 859 (1995).
[4] Y.-H. Kim, J. Opt. Soc. Am. B **20**, 1959 (2003).
[5] S.-Y. Baek, O. Kwon and Y.-H. Kim, Phys. Rev. A **77**, 013829 (2008).
[6] S. E. Harris, Phys. Rev. Lett. **98**, 063602 (2007).
[7] V. Balić, D. A. Braje, P. Kolchin and S. E. Harris, Phys. Rev. Lett. **94**, 183601 (2005).
[8] A. André, L.-M. Duan and M. D. Lukin, Phys. Rev. Lett. **88**, 243602 (2002).
[9] H. Schmidt and A. Imamoğlu, Opt. Lett. **21**, 1936 (1996).
[10] L.-M. Duan, M. D. Lukin, J. I. Cirac and P. Zoller, Nature (London) **414**, 413 (2001).
[11] S. Lloyd, M. S. Shahriar, J. H. Shapiro and P. R. Hemmer, Phys. Rev. Lett. **87**, 167903 (2001).
[12] K. F. Reim, J. Nunn, V. O. Lorenz, B. J. Sussman, K. C. Lee, N. K. Langford, D. Jaksch and I. A. Walmsley, Nat. Photonics **4**, 218 (2010).
[13] M. Hosseini, B. M. Sparkes, G. Campbell, P. K. Lam and B. C. Buchler, Nat. Commun. **2**, 174 (2011).
[14] Y.-W. Cho and Y.-H. Kim, Opt. Express **18**, 25786 (2010).
[15] Z. Y. Ou and Y. J. Lu, Phys. Rev. Lett. **83**, 2556 (1999).
[16] Y. J. Lu and Z. Y. Ou, Phys. Rev. A **62**, 033804 (2000).

[17] X.-H. Bao, Y. Qian, J. Yang, H. Zhang, Z.-B. Chen, T. Yang and J.-W. Pan, Phys. Rev. Lett. **101**, 190501 (2008).
[18] M. Scholz, L. Koch and O. Benson, Phys. Rev. Lett. **102**, 063603 (2009).
[19] C.-S. Chuu, G. Y. Yin and S. E. Harris, Appl. Phys. Lett. **101**, 051108 (2012).
[20] F. Wolfgramm, Y. A. de Icaza Astiz, F. A. Beduini, A. Cere and M. W. Mitchell, Phys. Rev. Lett. **106**, 053602 (2011).
[21] H. Zhang, X.-M. Jin, J. Yang, H.-N. Dai, S.-J. Yang, T.-M. Zhao, J. Rui, Y. He, X. Jiang, F. Yang, G.-S. Pan, Z.-S. Yuan, Y. Deng, Z.-B. Chen, X.-H. Bao, S. Chen, B. Zhao and J.-W. Pan, Nat. Photonics **5**, 628 (2011).
[22] C. H. van der Wal, M. D. Eisaman, A. Andre, R. L. Walsworth, D. F. Phillips, A. S. Zibrov and M. D. Lukin1, Science **301**, 196 (2003).
[23] A. Kuzmich, W. P. Bowen, A. D. Boozer, A. Boca, C. W. Chou, L.-M. Duan and H. J. Kimble, Nature **423**, 731 (2003).
[24] C. W. Chou, S. V. Polyakov, A. Kuzmich and H. J. Kimble, Phys. Rev. Lett. **92**, 213601 (2004).
[25] S. V. Polyakov, C. W. Chou, D. Felinto and H. J. Kimble, Phys. Rev. Lett. **93**, 263601 (2004).
[26] P. Kolchin, S. Du, C. Belthangady, G. Y. Yin and S. E. Harris, Phys. Rev. Lett. **97**, 113602 (2006).
[27] P. Kolchin, Phys. Rev. A **75**, 033814 (2007).
[28] S. Du. P. Kolchin, C. Belthangady, G. Y. Yin and S. E. Harris, Phys. Rev. Lett. **100**, 183603 (2008).
[29] Q.-F. Chen, B.-S. Shi, M. Feng, Y.-S. Zhang and G.-C. Guo, Opt. Express **16**, 21708 (2008).
[30] D.-S. Ding, Z.-Y. Zhou, B.-S. Shi, X.-B. Zou and G.-C. Guo, Opt Express **20**, 11433 (2012).
[31] S. Yun, J. Wen, P. Xu, M. Xiao and S.-N. Zhu, Phys. Rev. A **82**, 063830 (2010).
[32] J. Wen, Y.-H. Zhai, S. Du and M. Xiao, Phys. Rev. A **82**, 043814 (2010).
[33] J. F. Chen, S. Zhang, H. Yan, M. M. T. Loy, G. K. L. Wong and S. Du, Phys. Rev. Lett. **104**, 183604 (2010).
[34] S. Du, J. Wen, M. H. Rubin, J. Opt. Soc. Am. B **25**, C98 (2008).
[35] M. H. Rubin, D. N. Klyshko, Y. H. Shih and A. V. Sergienko, Phys. Rev. A **50**, 5122 (1994).
[36] Y. H. Shih, A. V. Sergienko, M. H. Rubin, T. E. Kiess and C. O. Alley, Phys. Rev. A **50**, 23 (1994).
[37] J. Wen, S. Du and M. H. Rubin, Phys. Rev. A **76**, 013825 (2007).
[38] B. L*ü*, W. H. Burkett and M. Xiao, Phys. Rev. A **56**, 976 (1997).
[39] M. Fleischhauer, A. Imamoglu and J. P. Marangos, Rev. Mod. Phys. **77**, 633 (2005).
[40] D. Felinto, C. W. Chou, H. deRiedmatten, S. V. Polyakov and H. J. Kimble, Phys. Rev. A **72**, 053809 (2005).
[41] O. Kwon, Y.-W. Cho and Y.-H. Kim, Phys. Rev. A **78**, 053825 (2008).